[1] **P Osman**[1]

**P V Sridevi** [2]

**K V S N Raju**[3]

# Design and Analysis of MIM Waveguide Based Refractive Index Sensor for Biomedical Applications

Journal of Electrical Systems

***Abstract:*** - This work deals with the characteristics of metal-insulator-metal waveguide and Stepped Impedance Resonator (SIR) based dual-band band pass filter (BPF) based sensor for biomedical applications are designed and analyzed using FDTD (finite differential time domain) solver-based CST studio suite software. MIMSIR biosensor is analyzed using APTES (3-aminopropyl triethoxysilane) and glucose is proposed in this work. The MIM characteristics of characteristic impedance and propagation lengths are analyzed. The MIMSIR is designed for 1274 nm (235.31 THz) and 1611 nm (186.09 THz) wavelengths. By incorporating glucose layer on MIM waveguide the resonating wavelengths of MIMSIR shifted to the right and the wavelengths observed are 1286 nm (233.12 THz) and 1631 nm (183.80 THz). APTES layer acts as linker between the organic to inorganic materials, by incorporating the APTES between the MIMSIR and Glucose layer the number of binding particles of the refractive index sensor increases and wavelength shifted to right side. The proposed MIMSIR-APTES-Glucose biosensor is operating in the frequency of 227.11 THz (1320 nm) and 177.81 THz (1686 nm) respectively. The sensitivity of the MIMSIR-APTES-Glucose sensor is demonstrated by its robust refractive index response, achieving 534.41 nm/RIU at 1320 nm and 855.83 nm/RIU at 1686 nm, showcasing its potential for accurate detection.

***Keywords:*** MIM, SIR, FDTD, APTES and Bio sensor.

## 1. Introduction

The advent of nano-plasmonics marks a substantial breakthrough in technology, enabling the circumvention of the diffraction limit and miniaturization of photonic integrated circuits (PICs) to nanoscale dimensions, paving the way for innovative applications [1]. At scales smaller than the wavelength of light, the limitations imposed by light waves are overcome by confining and guiding light through surface plasmons that propagate along metal-insulator-metal (MIM) waveguides, enabling subwavelength localization and manipulation of light. Unlike the principles of lossy conductors or ideal conductors used upto GHz frequencies, metals are characterized by lossy plasma behavior in nano-plasmonic systems. The propagation of surface waves along the interface between metal and insulator regions involves slow-wave in plasma, resulting in reduced phase velocity, shorter wavelengths, and higher wave impedance compared to conventional waves in the medium. These waves exhibit a mode similar to the TEM (transverse electromagnetic) mode, leading to the design of supporting structures resembling equivalent transmission lines. Various nanoplasmonic waveguiding structures, including IMI (insulator-metal-insulator) and MIM configurations, as well as nano-wires, have proposed to enable the realization of PICs (photonic integrated circuits) [2]. Among these structures, MIM waveguiding structures stand out due to their subwavelength characteristics and superior light confinement properties, making them ideal for such systems [4-14].

This area of research has seen significant development, particularly in the realm of nano sensors and PICs. Various advancements have led to the emergence of a novel technique involving MIM waveguide design and MIM based filters, couplers and biosensor are discussed in [15-19]. These MIM waveguides come in diverse geometries, each possessing unique properties such as refractive index (RI), bandwidth and resonant wavelength. By integrating silver baffles with the MIM ring cavity, it becomes possible to optimize sensitivity, with the observed 718

[1] * Corresponding author :**P Osman,** Department of Electronics and Communication Engineering, Dr. Samuel George Institute of Engineering &Technology, Darimadugu, Markapur, Prakasam-Dt, Andhra Pradesh, India, pathanosman@gmail.com.

2. **P V Sridevi**, Department of Electronics and Communication Engineering A U College of Engineering (A), Andhra University, Visakhapatnam, , Andhra Pradesh, India, pvs6_5@yahoo.co.in

3. **K V S N Raju**, Department of Electronics and Communication Engineering S.R.K.R. Engineering College, Bhimavaram , Andhra Pradesh, India. Kvsn45@gmail.com

nm/Refractive index unit (RIU) for optimum structure sensitivity was demonstrated in [20]. The refractive index (RI) stands out as a crucial parameter, essential for characterizing materials or solutions [21]. It serves as a measure of the composition and concentration of a solution, thus offering valuable insights into its properties with high precision [22-23]. Variations in the refractive index trigger a corresponding shift in the SIR characteristics, manifesting as changes in the resonance wavelength or angle, allowing for the quantitative determination of glucose concentration in the sample based on the magnitude of this shift. The section-2 presents the MIM waveguide characteristics and the MIM based SIR is analyzed for dual band BPF application is discussed in section-3 and MIMSIR based refractive index sensor is analyzed in section-4 using APTES and Glucose layers. The section-5 deals with the performance metrics of the biosensor and the paper ends with the conclusion in section-6.

## 2. MIM Waveguide Characteristics

The plasmonic MIM waveguide structure comprises two metal slabs separated by a dielectric material ($\varepsilon SiO2$ = 2.5) having a thickness (W), as depicted in the Fig. 1. The thickness of dielectric material ensures with deep subwavelength operations for single-mode of operation. By defining MIM waveguide properties like $n_{eff}$ (effective refractive index) and Zo. The two-wire transmission line model provides a suitable framework for designing and understanding the plasmonic MIM waveguide structure. The coupling of TM-polarized incident light into the waveguide induces Surface Plasmon Polaritons (SPPs) on the metal-insulator interface surfaces. Leveraging the established Drude model, silver is chosen as the metal, and its complex permittivity is characterized using the subsequent equation [14].

$$\varepsilon(m) = 1 - \frac{\omega_p^2}{\omega\left(\omega + i\gamma_p^2\right)} \qquad (1)$$

Where $\gamma_p = 2.73\times10^{13}$ rad/sec and $\omega_p = 1.38\times10^{16}$ rad/sec.

To simulate the MIM waveguide structure, perfectly matched layers (PML) boundary conditions are applied to the outer boundaries, excluding the input and output ports, as shown in Fig. 1. The propagation of the wave through the dielectric medium is characterized by a defined relationship for the characteristic impedance $Z_{PV} = V^2/P$, where $Z_{PV}$ depends on voltage and power, i.e., $Z_{PV} = V^2/P$.

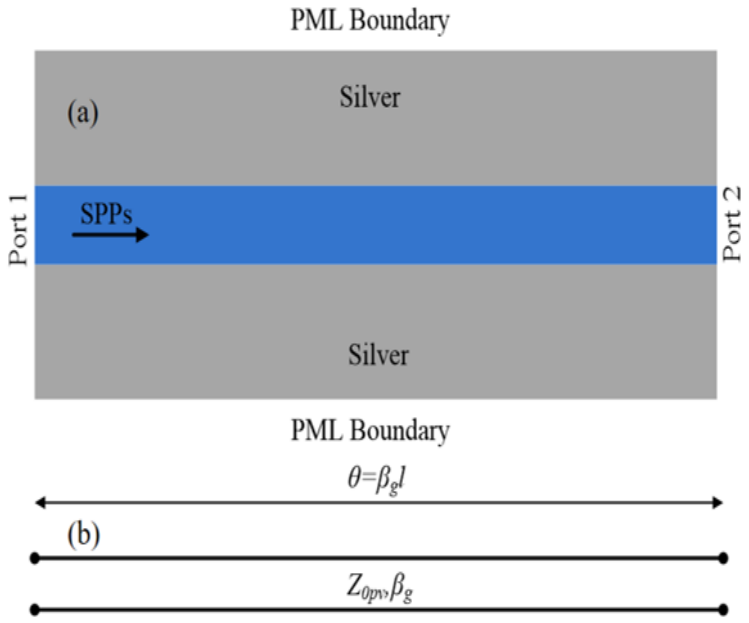


**Fig.1: (a) Schematic of nanoplasmonic MIM guiding structure and (b) Equivalent circuit of two wire Transmission Line**

Figure 2 illustrates the variation of the neff at different wavelengths i.e., 1350 nm and 1550 nm as a function of the insulator thickness (t). It can be observed from the figure that the neff increases as the dielectric width (W) decreases. Figure 3 displays the calculated equivalent $L_{spp}$(propagation length) derived from the simulation data.

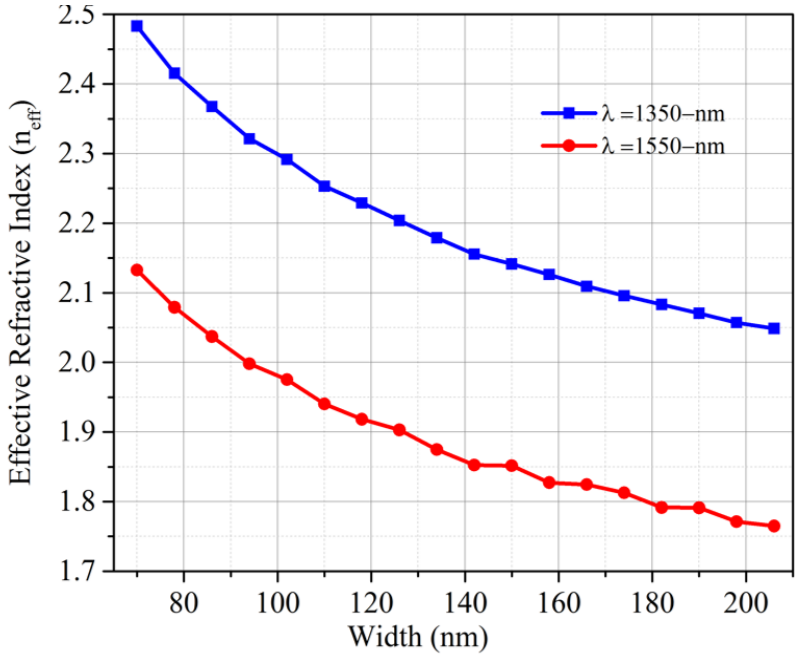


**Fig.2: Effective refractive index ($n_{eff}$) verses width (W) as a function of wavelengths 1350 nm and 1550 nm respectively**

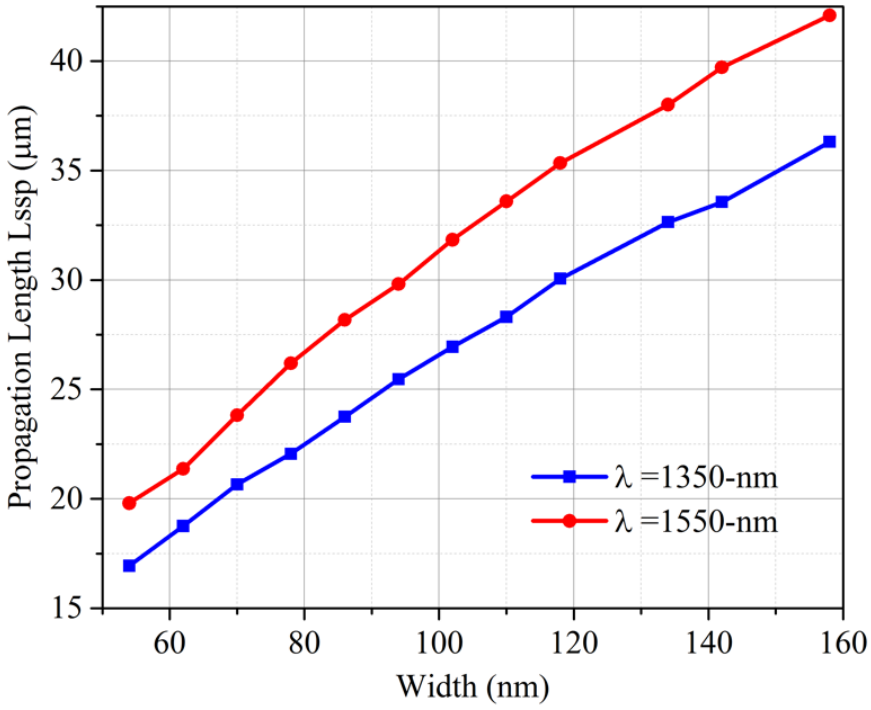


**Fig.3: Propagation length (Lspp) verses width (W) as a function of the wavelength at 1350 nm and 1550 nm respectively.**

Figure 4 illustrates the variation in characteristic impedance (Zo) at wavelengths of 1350 nm and 1550 nm as a function of waveguide width (W). A decrease in width (W) leads to an increase in characteristic impedance (Zo), with a maximum value of approximately 85 dB achieved at a width of 54 nm. Conversely, the propagation length exhibits a lower feasible value of less than 15 dB.

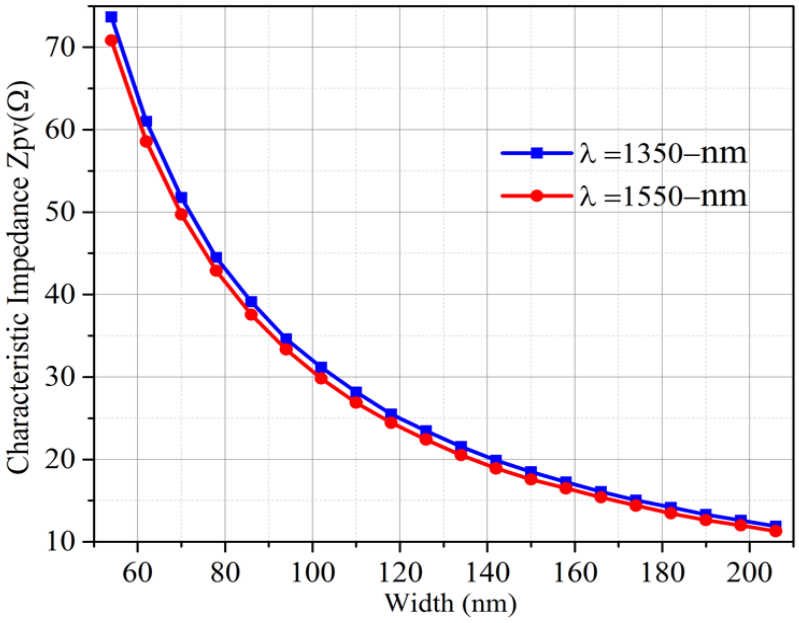


**Fig.4: Characteristic impedance verses width (W) as a function of wavelength 1350 nm and 1550 nm respectively.**

## 3. Design of MIM step impedance resonator filter (MIMSIR)

The proposed plasmonic MIM based Step impedance resonator (MIMSIR) schematic and its transmission line equivalent circuits are depicted in the Fig. 5, along with a comparison to [12]. The concept of λg/2 type MIM SIRs with even and odd modes was introduced by Jankovic et al. [15]. Each MIMSIR resonates in either the odd or even mode, with the fundamental resonant wavelength occurring in the odd-mode. The first higher-order resonant wavelength occurs, followed by subsequent resonances are observed in the even mode case. Thus, the conditions for the resonance are expressed as follows:

$$\tan\theta_2 = -R_Z \tan\theta_1 \quad \text{(even-mode)} \qquad (2)$$

$$\tan\theta_1 = R_Z \cot\theta_2 \quad \text{(odd-mode)} \qquad (3)$$

Where $R_Z = Z_2/Z_1 = \tan\theta_1 \tan\theta_2$(ration of impedances)

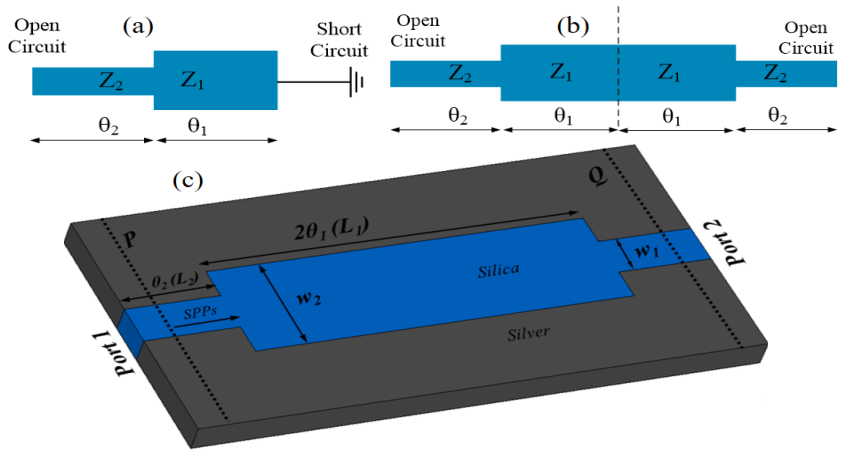


**Fig.5: Geometries of step impedance resonators (a) Quarter wavelength (b) Half wavelength (c) Plasmonic MIMSIR guiding structure.**

The resonance is depending on the electrical length of the resonators and the parameter Rz, the equivalent circuits of odd and even mode MIMSIR are analyzed for resonant frequencies. The fundamental resonance frequency with spurious frequency relationship is represented in the given equation.

$$\lambda \frac{f_{S1}}{f_0} = \frac{\pi}{2\tan^{-1}\sqrt{R_Z}} \quad (5)$$

$$\lambda \frac{f_{S2}}{f_0} = \frac{\pi}{\tan^{-1}\sqrt{R_Z}} \quad (6)$$

Where $f_{S1}$, $f_{S2}$and $f_0$are first, second and centre spurious frequencies respectively.

The proposed MIMSIR is designed and simulated using FDTD (Finite Differential Time Domain) solver-based CST studio suite software. For simulations the mesh size that considered is 5 nm X 5 nm along both co-ordinate directions i.e x and y. The TM mode of propagation is existed in the MIM waveguide, due to the W (width) of MIM waveguide is smaller than the wavelength. The MIMSIR structure design parameters are incorporated in table 1.

**Table 1. MIMSIR design parameters**

| S. No | Parameter | Value in nm |
|---|---|---|
| 1 | $L_1$ | 2020 |
| 2 | $L_2$ | 1010 |
| 3 | $W_1$ | 120 |
| 4 | $W_2$ | 420 |

The transmission and reflection coefficients of the proposed MIMSIR BPF is represented in figures 6 and 7 respectively. From the equation 5, the first and second resonances are occurred at 1611 nm (186.09 THz) and 1274 nm (235.31 THz). The figure 6 shows the variation of transmission and reflection coefficients with the parameter is L1 and the figure 7 represents the variation of the parameter W2. The variation of L1 provides the better impact comparing with the W2 parameter. MIMSIR two pass bands variation along with W2 parameter corresponding to the figure 6.

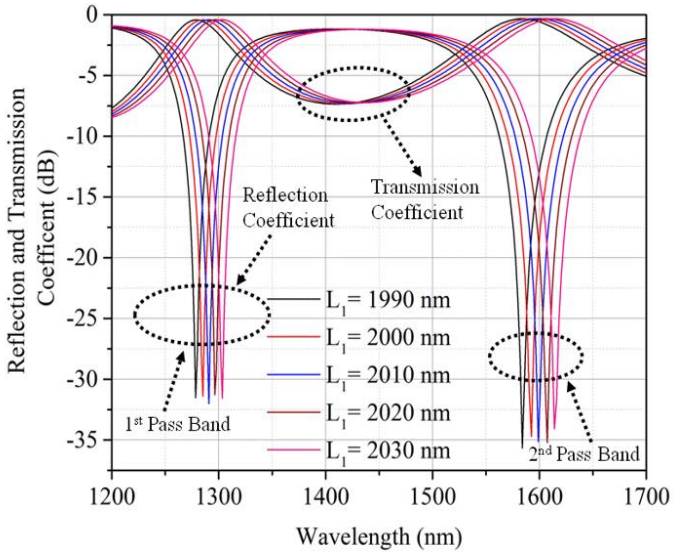


**Fig.6: Variation of reflection and transmission coefficients with wavelength as a function of Length (L1)**

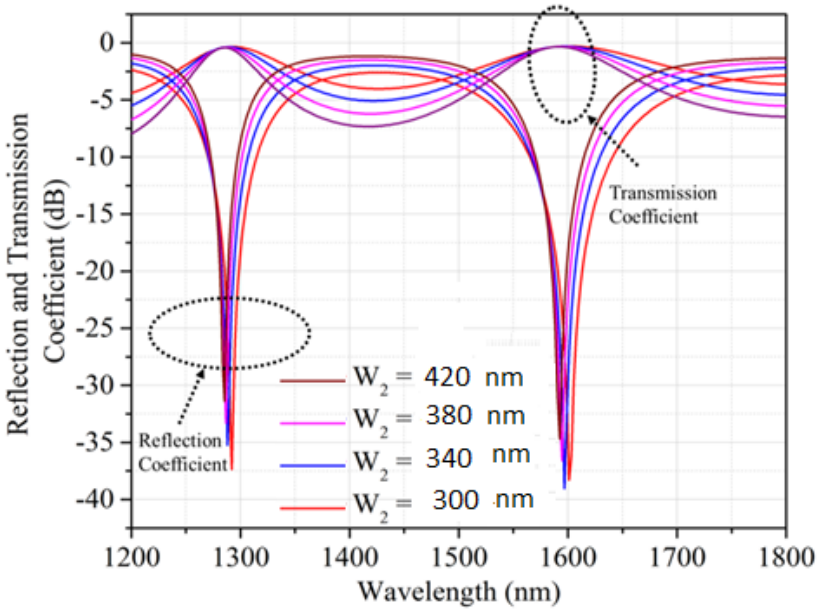


**Fig.7: Variation of reflection and transmission coefficient with wavelength as a function of width (W2)**

The E-field distributions of the proposed dual band filter is represented in figure 8 and the energy is mainly concentrated in the Metal and insulator regions.

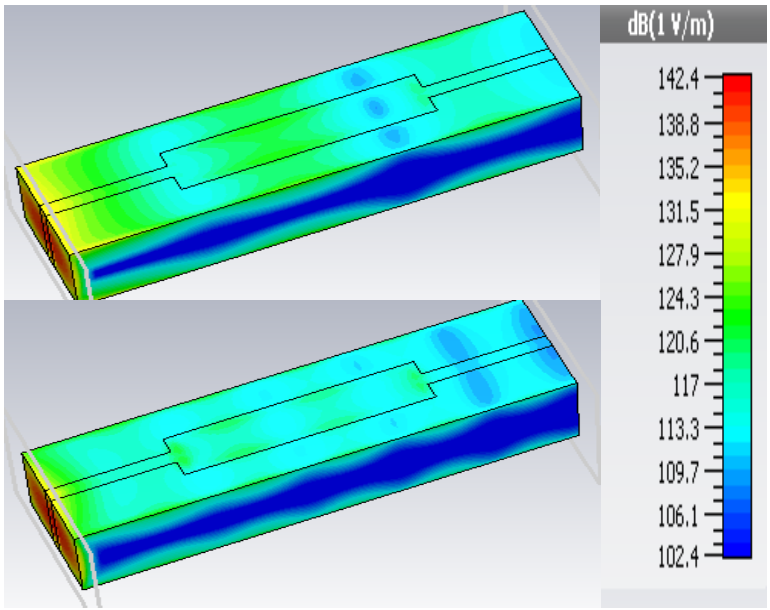


**Fig.8: Field distributions of MIMSIR at (a) 1274 nm (235.31 THz) and (b) 1611 nm (186.09)**

## 4. MIMSIR Refractive Index Sensor

The design procedure for the proposed biosensor utilizing MIMSIR is depicted in Figure 9. The SIR is coupled with MIM bus waveguides, are represented in the Figure 9 (a). The figure 9(b) illustrates the MIMSIR with a single layer of Glucose (MIMSIR-Glucose) coated on the SIR, with the Glucose material represented in violet colour in figure 9. In the proposed structure, APTES served as a bridging layer, enabling the covalent attachment of organic biomolecules to the

inorganic surface through an adsorption reaction, and thus establishing a robust link between the organic and inorganic domains.

The proposed biosensor combines APTES and Glucose layers on the MIMSIR and it denoted as MIMSRR-

APTES-Glucose with APTES depicted in purple in Figure 9(c). The refractive index of Glucose is 1.33 and APTES was 1.413 respectively. In the simulation environment, the thickness of both the glucose layer and the APTES layer was assumed to be 5 nm each, allowing for a consistent and controlled interface between the organic and inorganic regions.

Figure 10 presents the transmission and reflection coefficients of the biosensor. To assess the biosensing capabilities of the proposed biosensor structures, a study was conducted to examine how changes in refractive index (RI) caused by different biomaterials (APTES and Glucose) affect the wavelength shift in the reflection parameter, thereby evaluating the sensor's response to varying biomaterial properties. It demonstrates a minimal shift in wavelengths to the right for MIMSIR-Glucose and MIMSIR-APTES-Glucose

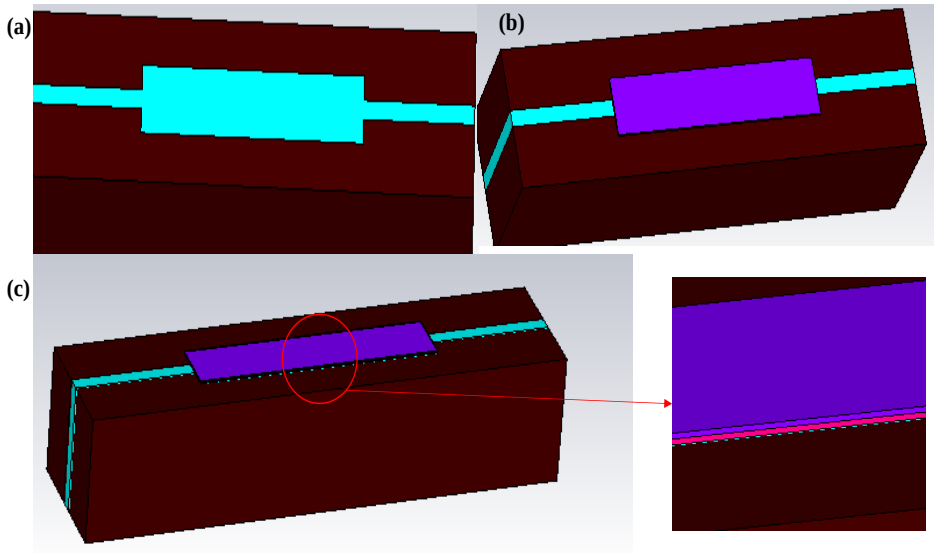


**Fig.9: Schematic diagrams of (a) MIMSIR (b) MIMSIR-Glucose (c) MIMSIR-APTES-Glucose.**

The resonating wavelengths for the proposed MIMSIR are 1274 nm (235.31 THz) and 1611 nm (186.09 THz) respectively. The resonating wavelengths of MIMSIR-Glucose are 1286 nm (233.12 THz) and 1631 nm (183.80 THz). A linker layer of APTES is sandwiched between the MIMSIR-Glucose layers. APTES serves as a bridge between organic and inorganic surfaces, facilitating molecular interactions and enhancing conductivity by generating electrical signals. The proposed MIMSIR-APTES-Glucose device benefits from an increased surface-to-volume ratio, leading to improved sensitivity. Reflection and transmission coefficients for MIMSIR-APTES-Glucose are depicted in Figure 10. By incorporating APTES, the wavelength shifts from 1274 to 1320 nm, and from 1611 nm to 1686 nm.

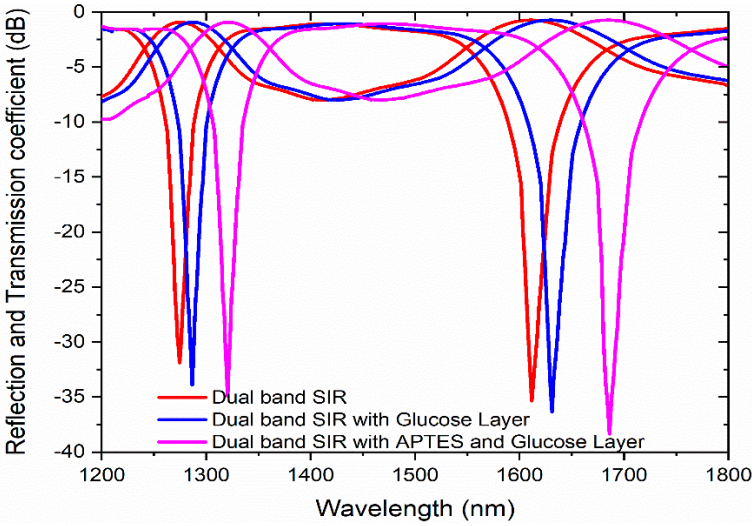


**Fig. 10: Reflection and Transmission coefficient of MIMSIR, MIMSIR-Glucose and MIMSIR-APTES-**

**Glucose**

The E-field distributions of the proposed MIMSIR-Glucose and MIMSIR-APTES-Glucose are represented in figure 11(a) and (b) respectively. By inclusion of APTES layer in the Metal and glucose layer the interaction of molecules increases and E field concentration increases and represented in figure 11(b).

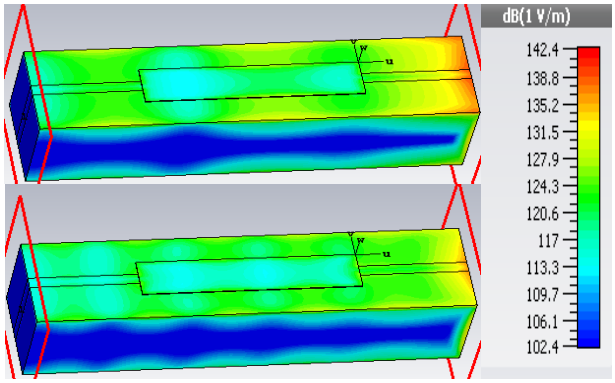


(a)

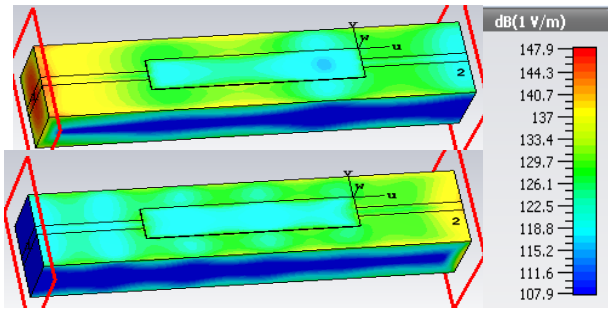


(b)

**Fig.11: E-field distributions (a) MIMSIR-Glucose at 1286 nm and 1631 nm (b) MIMSIR-APTES-Glucose at the resonating wavelengths of 1320 nm and 1686 nm**

## 5. Performance Metrix of proposed MIMSIR

The performance of proposed SIR using Q-factor, FSR (Free spectral range), ER (Extinction ratio), Finence and FWHM (Full width half maximum). ER represents the ratio of minimum to maximum transmission outputs. FWHM and FSR are dependent on the resonating wavelength ( $\lambda$ ). The difference between two resonance wavelengths is represented by FSR [24]. The Q-factor is (resonant wavelength/FWHM).

$$FSR=\lambda^2/n_g L \quad (7)$$

Finence denoted by the ratio FSR/FWHM, serves as a measure of sharpness relative to the spacing between resonance peaks, while the sharpness relative to the resonating wavelength is measured using Q-factor [24].

$$S = \Delta \lambda_{resonance}/\Delta n \quad (8)$$

The Figure of Merit (FOM) of the proposed sensor was computed using below equation [14].

$$FOM = S/FWHM \quad (9)$$

The parameters of the MIMSIR, MIMSIR-Glucose and MIMSIR-APTES-Glucose are ER, FWHM, FSR, Q-factor, Finence, FOM and Sensitivity are calculated using the formulas indicated in the equations 7-9 and the comparison of all the parameters are tabulated in table 2 i.e spectral analysis of proposed refractive index sensor (RIS).

**Table 2: Spectral analysis for the proposed RIS**

| *Parameters* | *MIMSIR* | *MIMSIR-Glucose* | *MIMSIR-APTES-Glucose* |
|---|---|---|---|
| **ER (dB)** | 32 | 34 | 36 |
| **FWHM (nm)** | ~28& ~52 | ~29 & ~51 | ~29 & ~57 |
| **FSR (nm)** | 337 | 341 | 347 |
| **Q-Factor** | 45.5 & 30.9 | 44.31 & 31.9 | 45.51&29.6 |
| **Finence** | 12.03 & 6.48 | 11.75 & 6.48 | 11.96 & 6.08 |
| **Sensitivity (nm/RIU)** | NA | 121.33 & 195.32 | 534.41 & 855.83 |
| **FOM** | NA | 4.18 & 3.83 | 18.42 & 15.01 |

The sensitivity of the MIMSIR-APTES-Glucose is more by comparing with MIMSIR-Glucose due to more surface currents produced because of more bonding of the Glucose particles. Table 3 represents the sensitivity of the proposed glucose sensor is compared with the previous literature.

**Table 3: Comparison of proposed structure with previous literature**

| *S.NO* | *Reference* | *Wavelength (nm)* | *Structure* | *Sensitivity (nm/RIU)* |
|---|---|---|---|---|
| **1** | [20] | 710 | Ring | 718 |
| **2** | [25] | 780 | Rectangular | 750 |
| **3** | [26] | 1560 | Hybrid-Plasmonic Waveguide | 800 |
| **4** | [27] | 838.87 and 1609.7 | rectangular | 303.72 (first resonance) & 783.61 (second resonance) |
| **5** | [28] | 571 | Hexagonal | 550 |
| **6** | [29] | 1050 and 1750 | Unit cell | 585.277 (first resonance) & 652.777 (second resonance) |
| **7** | [30] | | Ring | 206 |
| Proposed | | 1320 and 1686 | MIMSIR | 534.41 (first resonance) & 855.83 (second resonance) |

Based on the enhanced electromagnetic fields at the metal surface the proposed plasmonic refractive sensor can detect very low concentrations of glucose, making them highly sensitive and suitable for medical diagnostics, including continuous glucose monitoring for diabetes management. Overall, plasmonic glucose sensors offer a promising approach for accurate, sensitive, and real-time glucose monitoring.

## 6. Conclusion

In this paper, the characteristics of MIM waveguide was numerically analyzed by using the parameters characteristic impedance and propagation length. The MIM based stepped impedance resonator filter (MIMSIR) is investigated for dual bandpass filter application. The BPF is converted to biosensor by incorporating the glucose layer on top of the SIR. The detection of glucose molecules increased by including the APTES layer (linker layer) between SIR and glucose layers, observing the more currents are generated by incorporating APTES layer with

the thickness of 5 nm each. Because of APTES the resonating wavelengths are shifted towards right. The sensitivity is 534.41nm/RIU and 855.83nm/RIU, the FOM is 18.42 and 15.01. The proposed refractive index-based biosensor is suitable for glucose detection with its good sensitivity.

**Acknowledgement**

The authors acknowledge support by the Andhra University, Vishakhapatnam, and Andhra Pradesh, India.

## REFERENCES

[1] R. Zia, M. D. Selker, P. B. Catrysse, and M. L. Brongersma, “Geometries and materials for subwavelength surface plasmon modes,” J. Opt. Soc. Am. A, vol. 21, no. 12, pp. 2442-2446, July 2004.

[ 2] Z. Han, “Ultracompact plasmonic racetrack resonators in metal-insulator-metal waveguides,” Photonics Nanostructures - Fundam. Appl., vol. 8, no. 3, pp. 172-176, Apr. 2010.

[3] S. Mokkapati, D. Saxena, N. Jiang, H. H. Tan, and C. Jagadish, “Plasmonic cavities for increasing the radiative efficiency of GaAs nano wires,” 2014 Conf. Optoelectron. Microelectron. Mater. Devices, commad 2014, vol. 1, pp. 244-245, Dec. 2014.

[4] J. Qi et al., “Independently tunable double Fano resonances in asymmetric MIM waveguide structure,” Opt. Express, vol. 22, no. 12, pp. 14688-14695, Jun. 2014.

[5] Xian-Shi Lin and Xu-Guang Huang, “Tooth-shaped plasmonic waveguide filters with nanometeric sizes 1,” Opt. Lett., vol. 33, no. 23, pp. 2874-2876, Dec. 2008.

[6] A. M. Heikal, M. F. O. Hameed, and S. S. A. Obayya, “Coupling characteristic of a novel hybrid long-range plasmonic waveguide including bends,” IEEE J. Quantum Electron., vol. 49, no. 8, pp. 621-627, Aug. 2013.

[7] L. Wu, P. Bai, X. Zhou, and E. P. Li, “Reflection and transmission modes in nanohole-array-based plasmonic sensors,” IEEE Photonics J., vol. 4, no. 1, pp. 26-33, Feb. 2012.

[8] J. Gosciniak, L. Markey, A. Dereux, and S. I. Bozhevolnyi, “Thermo-optic control of dielectric-loaded plasmonic Mach-Zehnder interferometers and directional coupler switches,” Nanotechnology, vol. 23, no. 44, pp. 444008 (1-9), Oct. 2012.

[9] S. Zhu, H. S. Chu, G. Q. Lo, and D. L. Kwong, “CMOS-compatible plasmonic bragg reflectors based on cu-dielectric-si structures,” IEEE Phot. Tech. Lett., vol. 25, no. 21, pp. 2115-2118, Nov. 2013.

[10] Y. B. Zheng, et. al, “Incident-angle-modulated molecular plasmonic switches: A case of weak exciton-plasmon coupling,” Nano Lett., vol. 11, no. 5, pp. 2061-2065, Apr. 2011.

[11] V. Liu, Y. Jiao, D. A. B. Miller, and S. Fan, “Design methodology for compact photonic-crystal-based wavelength division multiplexers,” Opt. Lett., vol. 36, no. 4, pp. 591-593, Feb. 2011.

[12] Ravi Kiran Chityala, “Nanoplasmonic concurrent dual band antennas using metal-insulator-metal step impedance resonators,” Microwave and Optical Tech. Lett., Feb.2019.

[13] K. Thirupathaiah, B. Iyer, N. Prasad Pathak, and V. Rastogi, “Concurrent dualband diplexer for nanoscale wireless links,” IEEE Photonics Technol. Lett., vol. 26, no. 18, pp. 1832-1835, Sep. 2014.

[14] K. R. Hiremath, L. Zschiedrich, and F. Schmidt, “Numerical solution of nonlocal hydrodynamic Drude model for arbitrary shaped nano-plasmonic structures using Nédélec finite elements,” J. Comput. Phys., vol. 231, no. 17, pp. 5890-5896, May 2012.

[15] J. Tao, Q. J. Wang, and X. G. Huang, “All-optical plasmonic switches based on coupled nano-disk cavity structures containing nonlinear material”, Plasmonics, vol. 6, no. 4, pp. 753, Aug. 2011.

[16] H. Lu, X. Liu, D. Mao, and G. Wang, “Plasmonic nanosensor based on fano resonance waveguide-coupled resonators”, Opt. lett., vol. 37, no. 18, pp. 3780–3782, Sep. 2012.

[17] G. Wang, H. Lu, X. Liu, D. Mao, and L. Duan, “Tunable multi-channel wavelength demultiplexer based on mim plasmonic nanodisk resonators at telecommunication regime”, Opt. Express, vol. 19, no. 4, pp. 3513– 3518, Feb. 2011.

[18] H. Lu, X. Liu, Y. Gong, D. Mao, and L. Wang, “Enhancement of transmission efficiency of nanoplasmonic wavelength demultiplexer based on channel filters and reflection nanocavities”, Opt. express, vol. 19, no. 14, pp. 12885–12890, Jul. 2011.

[19] Y. Gong, L. Wang, X. Hu, X. Li, and X. Liu, “Broad-bandgap and lowsidelobe surface plasmon polariton reflector with bragg-grating-based mim waveguide”, Opt. Express, vol. 17, no. 16, pp. 13727–13736, Aug. 2009.

[20] X. Zhao, Z. Zhang, and S. Yan, “Tunable fano resonance in asymmetric mim waveguide structure”, Sensors, vol. 17, no. 7, pp. 1494, Jun. 2017.

[21] C.Y. Tan and Y. X. Huang, "Dependence of Refractive Index on Concentration and Temperature in Electrolyte Solution, Polar Solution, Nonpolar Solution, and Protein Solution", J.Chem.Eng.Data, Vol.60, no.10, pp.2827-2833, Sep. 2015.

[22] M. Bertolotti, V. Bogdanov, A. Ferrari, A. Jascow, N. Nazorova, A. Pikhtin, and L. Schirone, "Temperature dependence of the refractive index in semiconductors", Opt. Express, Vol. 7, No. 6, pp.918-922, Mar. 1990.

[23] V. K. singh, V. Kumar, et.al., "Application of He-Ne Laser to Study of the Variation of Refractive Index of Liquid Solutions with the Concentration", J. Integr. Sci. Technol., Vol. 1, no. 1, pp. 13-18, May. 2013.

[24] W. Bogaerts et.al., “Silicon Microring Resonators”, Lasers and Photonics Review, vol. 6, pp. 47-73, 2012.

[25] S. Pang, Y. Huo, Y. Xie, and L. Hao, “Fano resonance in mim waveguide structure with oblique rectangular cavity and its application in sensor”, *Opt. Comm*., vol. 381, pp. 409–413, Jul. 2016.

[26] M. Butt, S. Khonina, and N. Kazanskiy, “Hybrid plasmonic waveguideassisted metal–insulator–metal ring resonator for refractive index sensing”, *J. Mod. Opt., vol.* 65, no. 9, pp. 1135–1140, Jan. 2018.

[27] M. F. Hassan, M. M. Hasan, M. Radoan and R. H. Sagor, "Design and Performance Analysis of an Ultra-compact Nano-plasmonic Refractive Index Sensor," 2020 8th International Electrical Engineering Congress (iEECON), pp. 1-5, 2020.

[28] C. Wu, H. Ding, T. Huang, et.al., "Plasmon-Induced Transparency and Refractive Index Sensing in Side-Coupled Stub-Hexagon Resonators", *Plasmonics*, Vol. 13, pp. 251–257, Feb. 2018.

[29] Z. Madadi, K. Abedi, G. Darvish, et.al., "Dual-wavelength plasmonic perfect absorber suitable for refractive index sensing", Plasmonics, Vol. 15, pp. 703–708, Jun. 2020.

[30] sourabh sahu,[1] nitesh mudgal,[2,3] ankit agrawal,[3] and ghanshyam singh[3] “detection of biomolecules and glucose concentration in bloodusing a subwavelength grating optical biosensor”hindawi journal of sensors ,volume 2023, article id 5533918, 7 pages, 11 august 2023